

Proposal to use superparamagnetic nanoparticles to test the role of cryptochrome in magnetoreception

Susannah Bourne Worster¹ and P. J. Hore^{1,*}

¹ Department of Chemistry, University of Oxford, Physical and Theoretical Chemistry Laboratory, South Parks Road, Oxford OX1 3QZ, U.K.

* Author for correspondence: peter.hore@chem.ox.ac.uk

Keywords

cryptochrome, magnetic field effect, magnetic nanoparticle, magnetoferritin, magnetoreception, radical pair mechanism,

Abstract

Evidence is accumulating to support the hypothesis that some animals use light-induced radical pairs to detect the direction of the Earth's magnetic field. Cryptochrome proteins seem to be involved in the sensory pathway but it is not yet clear if they are the magnetic sensors: they could, instead, play a non-magnetic role as signal transducers downstream of the primary sensor. Here we propose an experiment with the potential to distinguish these functions. The principle is to use superparamagnetic nanoparticles to disable any magnetic sensing role by enhancing the electron spin relaxation of the radicals so as to destroy their spin correlation. We use spin dynamics simulations to show that magnetoferritin, a synthetic, protein-based nanoparticle, has the required properties. If cryptochrome is the primary sensor, then it should be inactivated by a magnetoferritin particle placed 12-16 nm away. This would prevent a bird from using its magnetic compass in behavioural tests and abolish magnetically sensitive neuronal firing in the retina. The key advantage of such an experiment is that any signal transduction role should be completely unaffected by the tiny magnetic interactions ($\ll k_B T$) required to enhance the spin relaxation of the radical pair.

1. Introduction

Since it was first demonstrated in the 1960s that migratory birds can sense the direction of the geomagnetic field [1, 2], the quest to uncover the underlying biophysical mechanism has been hampered by the lack of an unambiguously identified receptor [3, 4]. Although it had been proposed in 1978 that radical pairs could be the magnetically sensitive entities [5], their identity remained obscure until 2000 when the protein cryptochrome was proposed as a potential light-dependent magnetoreceptor [6]. Subsequent work [7-12] suggests that cryptochromes are well-suited for this purpose (reviewed in [13-15]). The sensors are located in the birds' retinas, which contain four different cryptochromes (1a, 1b, 2 and 4) [16-20]. Of these, cryptochrome 4, present in the outer segments of the double-cone photoreceptor cells, is the most likely to be a magnetic sensor [20]. Other studies suggest that cryptochromes also mediate a variety of magnetic responses in insects [21-29]. However, although there is appreciable evidence that cryptochrome plays a role of some kind in magnetoreception, there is still no proof that it is the sensor rather than, for example, an essential downstream component in the magnetic signal transduction pathway [15] or an upstream regulator of the magnetic sensor.

Elucidation of the magnetic function of cryptochrome *in vivo* requires a carefully designed experiment in which the magnetic properties of the protein can be selectively modified without otherwise affecting its ability to participate in a sensory pathway. Site-specific mutations are unlikely to satisfy this condition. Although amino acid substitutions could, for example, prevent radical pair formation [22, 30, 31] and so abolish magnetic sensing, they may also induce structural and dynamical changes that would obstruct a signal transduction role. Fortunately, detection of magnetic fields via the radical pair mechanism depends on the delicate interplay of magnetic interactions that are orders of magnitude weaker than those that govern chemical bonding, molecular structure and reaction kinetics, providing an extremely gentle and potentially selective way to disrupt the operation of a radical pair compass sensor [15].

According to the radical pair mechanism, the direction of an external magnetic field can be determined via its influence on the dynamics of the interconversion between singlet (antiparallel electron spins) and triplet (parallel electron spins) states of two light-induced, spin-correlated radicals [5]. A consequence of their photochemical origin is that the radical pairs in cryptochrome are created in a pure singlet state, far removed from the 1:3 singlet:triplet ratio expected for thermal equilibrium [12, 32]. If the radicals remain in a coherent, non-equilibrium state for about 1 μ s, then, in principle, the interaction of the electron spins with the geomagnetic field can modify the spin dynamics and hence alter the yields of the reaction products [15, 33]. If the spins relax too quickly, all information about the magnetic field is lost [34-36].

In this report, we propose an experiment in which a cryptochrome-based magnetic compass sensor could be selectively disabled by attaching a superparamagnetic nanoparticle as a spin

relaxation agent. Although the context is very different, the principle is not unlike that of the contrast agents used in magnetic resonance imaging (MRI) [37-39]. Section 2 outlines the model used to simulate the destructive influence of the fluctuating magnetic field of the nanoparticle on a nearby radical pair. Our approach differs fundamentally from previous theoretical work in this area, which focussed on the magnetic amplification effect of, for example, coherent spin evolution driven by the magnetic field gradient of a nearby single-domain magnetite crystal [40-43]. The following section reports simulations designed to determine the optimum timescale (Section 3.1) and strength (Section 3.2) of the fluctuating field and hence how close the nanoparticle would need to be to induce significant spin relaxation in the radical pair. Section 3.3 discusses the choice of nanoparticle, Section 3.4 discusses some practical considerations and Section 3.5 outlines preliminary *in vitro* experiments that could be used to validate the approach and quantify the relaxation enhancement.

2. Methods

The key characteristic of a superparamagnetic nanoparticle is that its magnetic moment is unstable and changes direction with a characteristic time constant known as the Néel relaxation time, τ_N . Such particles are therefore the source of a fluctuating local magnetic field that could potentially relax the electron spins of a nearby radical pair and so degrade its sensitivity to an external magnetic field. Spin relaxation can also result from the Brownian motion of the nanoparticle if it modulates the distance to the radicals and hence the magnetic field they experience.

The Néel relaxation of a superparamagnetic nanoparticle with strong uniaxial symmetry involves virtually instantaneous flips of its magnetic moment between two antiparallel orientations aligned with the ‘easy axis’ of the particle. A strong external magnetic field can bias these fluctuations such that the magnetic moment becomes polarized in the direction of the field. However, in an Earth-strength field ($\sim 50 \mu\text{T}$) at physiological temperatures, the degree of alignment is $\sim 10^{-7}(\mu_{\text{NP}} / \mu_B)$ [44], where μ_{NP} is the instantaneous magnetic moment of the nanoparticle and μ_B is the Bohr magneton. Therefore, for magnetic moments smaller than $\sim 1000\mu_B$ (see later), the two orientations are almost equally likely and the time between flips is exponentially distributed with a mean value τ_N . This behaviour can be captured by a model in which the system jumps between two equally populated sites, A and B, corresponding to the two orientations of the magnetic moment. The spin dynamics of a radical pair subject to the magnetic field of a nearby nanoparticle can therefore be described by two coupled Liouville-von Neumann equations [9, 45]:

$$\frac{d}{dt} \begin{pmatrix} \hat{\rho}_A(t) \\ \hat{\rho}_B(t) \end{pmatrix} = \begin{pmatrix} -\hat{L}_A - \hat{1}/\tau_N & \hat{1}/\tau_N \\ \hat{1}/\tau_N & -\hat{L}_B - \hat{1}/\tau_N \end{pmatrix} \begin{pmatrix} \hat{\rho}_A(t) \\ \hat{\rho}_B(t) \end{pmatrix} = -\hat{L} \begin{pmatrix} \hat{\rho}_A(t) \\ \hat{\rho}_B(t) \end{pmatrix}, \quad (2.1)$$

where $\hat{\rho}_j(t)$ is the spin density operator for site j ($= A, B$), $\hat{1}$ is the identity superoperator and the \hat{L}_j are the two Liouvillian superoperators:

$$\hat{L}_j \hat{\rho}_j(t) = i[\hat{H}_0 + \hat{H}_j, \hat{\rho}_j(t)] + k \hat{\rho}_j(t). \quad (2.2)$$

The spin Hamiltonian, \hat{H}_0 , contains the interactions of the two electron spins with the geomagnetic field and with the nuclear spins in each radical (hyperfine interactions). \hat{H}_A and \hat{H}_B in equation (2.2) represent the Zeeman interactions of the electron spins with the fields produced by the two orientations of the nanoparticle's magnetic moment. The singlet and triplet states of the radical pair are assumed to react spin-selectively with the same rate constant, k , to give distinct products [46]. The fractional yield of the product formed from the singlet state, which we shall call the 'singlet yield', $\Phi_s(\theta)$, is calculated as [9]

$$\Phi_s(\theta) = \frac{k}{Z} (\hat{P}^s \hat{P}^s) \hat{L}^{-1} \begin{pmatrix} \hat{P}^s \\ \hat{P}^s \end{pmatrix}, \quad (2.3)$$

where \hat{P}^s is the singlet projection operator, Z is twice the number of nuclear spin states in the radical pair, and θ is the angle between the axis of the 50 μT external magnetic field and the z-axis of the radical pair (figure 1). The radical pair is assumed to be created in a pure singlet state. The same approach may be used as a crude model of the Brownian motion of the particle by allowing it to hop back and forth between two equally populated sites at different distances from the radicals (see figure 1). In this case τ_N is replaced by τ_B , the average time between jumps. Further details can be found in the Supplementary Information. The nanoparticle is treated as a point magnetic dipole generating a magnetic field that falls off as r^{-3} , where r is the distance from the centre of the particle. The two radicals therefore experience different magnetic fields (although the effect of this difference proved to be minor).

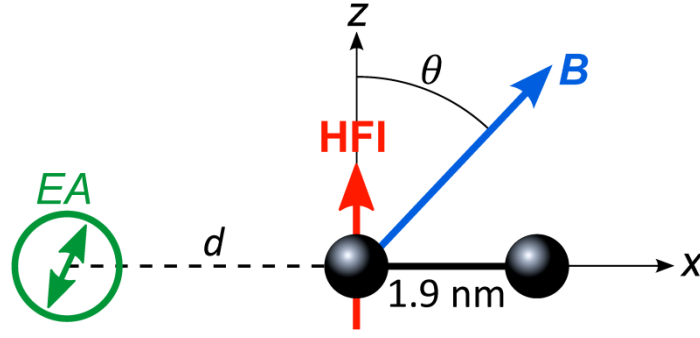


Figure 1. Arrangement of the radicals (black spheres) and nanoparticle (green circle) in the toy model. The “primary” radical, which contains the magnetic nucleus, is placed at the origin; the symmetry axis of its hyperfine interaction (**HFI**, red arrow) defines the z-axis. The “secondary” radical is 1.9 nm away along the x-axis. The nanoparticle is at a distance d from the primary radical, also on the x-axis. In the toy model, the easy axis of the nanoparticle (**EA**, green arrow) is parallel to either the x- or the z-axis. The direction of the geomagnetic field (**B**), defined by the angle θ , is in the xz-plane. Brownian motion was modelled by allowing the nanoparticle to jump from the position shown to either $(x, z) = (-d - \Delta d, 0)$ (x-axis hops) or $(x, z) = (-d, \Delta d)$ (z-axis hops).

3. Results

3.1 Néel relaxation time of the nanoparticle

Criteria for selecting a suitable nanoparticle can be derived by modelling a toy radical pair containing a single spin- $\frac{1}{2}$ nucleus (e.g. ^1H) in one of the radicals, with a recombination lifetime (k^{-1}) of 10 μs . For simplicity, the hyperfine tensor was chosen to be axially symmetric with principal values $(A_{xx}, A_{yy}, A_{zz}) = (0.0, 0.0, 1.5)$ mT. The radicals are 1.9 nm apart (to match the separation of the magnetically sensitive radicals in cryptochrome [47, 48]) and the nanoparticle is placed on the inter-radical axis, $d = 12$ nm from the (“primary”) radical that carries the nuclear spin and 13.9 nm from the (“secondary”) radical (figure 1). Equation (2.3) was used to calculate the singlet yield anisotropy, defined as $\Delta\Phi_s = \Phi_s(0) - \Phi_s(90^\circ)$, the difference in the singlet yields when the geomagnetic field is parallel and perpendicular to the hyperfine axis. As in previous studies [8, 9], we assume that $\Delta\Phi_s$ quantifies the sensitivity of the compass to changes in the direction of the geomagnetic field.

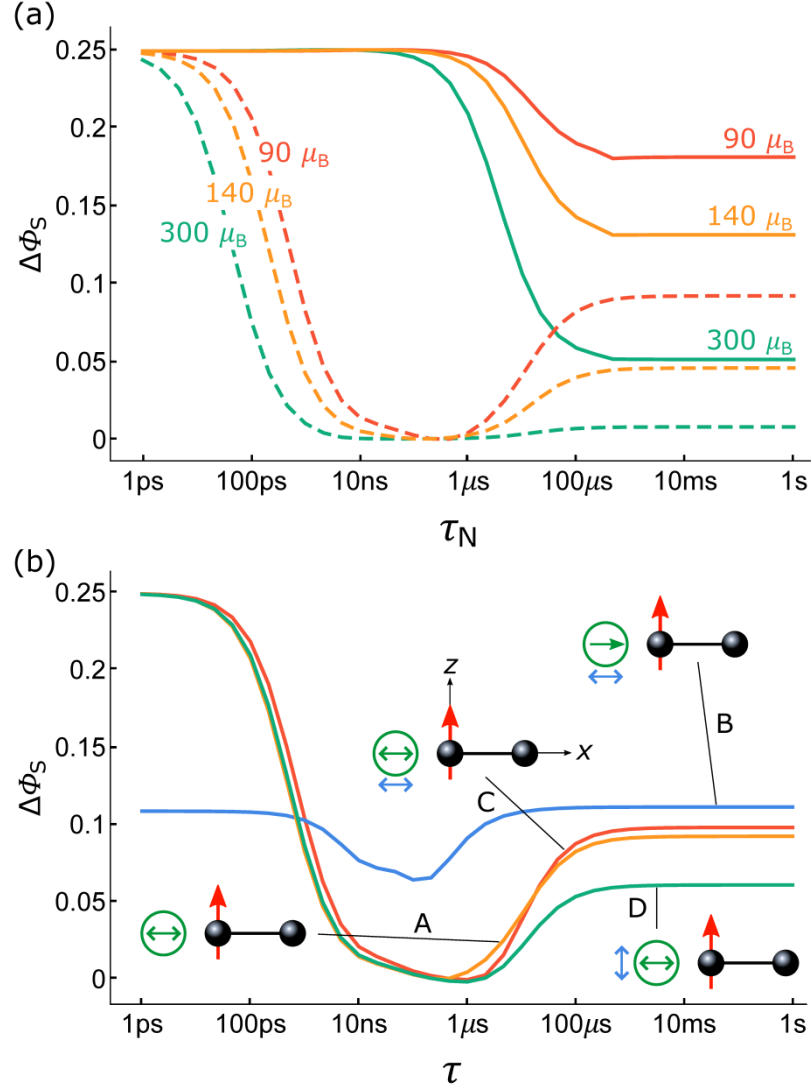


Figure 2. Singlet yield anisotropy ($\Delta\Phi_s$) for a toy radical pair containing a single spin- $\frac{1}{2}$ nucleus. (a) The dependence of $\Delta\Phi_s$ on the Néel relaxation time (τ_N), the magnetic moment of the nanoparticle (values selected from Ref. [49]) and the orientation of the easy axis of the nanoparticle, which is either parallel (solid lines) or perpendicular (dashed lines) to the principal axis of the hyperfine interaction in the radical pair (the z-axis in figure 1). (b) The variation of the anisotropy when the nanoparticle is performing one of the following combinations of Néel relaxation (with the easy axis perpendicular to the principal axis of the hyperfine interaction) and 2 nm hops (to model Brownian motion): (A) Néel relaxation ($\tau = \tau_N$) only; (B) x-axis hopping ($\tau = \tau_B$) only; (C) x-axis hopping ($\tau_B = 1$ ns) and Néel relaxation ($\tau = \tau_N$); (D) z-axis hopping ($\tau_B = 1$ ns) and Néel relaxation ($\tau = \tau_N$). (C) and (D) were calculated using a four-site model (see Supplementary Information). The magnetic moment of the nanoparticle was taken as $90\mu_B$. Black sphere: radical. Green circle: nanoparticle. Red arrow: symmetry axis of the hyperfine interaction. Green arrow: easy axis of the nanoparticle. Blue arrow: nanoparticle hopping motion.

Figure 2(a) shows the variation of $\Delta\Phi_s$ with τ_N for three magnetic moments and two orthogonal easy-axis directions. For this very simple radical pair, the effect of the nanoparticle depends strongly on the direction of the easy axis relative to the hyperfine axis: no relaxation is induced when these axes are parallel (solid lines) and the relaxation is most efficient when they are perpendicular (dashed lines). This distinction is less marked for a more realistic radical pair containing several hyperfine interactions in both radicals (see below and Supplementary Information). In practice, the easy axis would be randomly oriented relative to the molecular frame of the radical pair, making this difference largely irrelevant. The parallel configuration is included in figure 2(a) for comparative purposes, to show how $\Delta\Phi_s$ depends on τ_N in the absence of spin relaxation.

The effect of the nanoparticle depends strongly on its Néel relaxation time (figure 2(a)). For very fast flipping ($\tau_N < 1$ ps) there is no effect at all: the spins of the radicals cannot react to such a rapidly switching magnetic field. In the other extreme, when the flipping is very slow ($\tau_N > 1$ ms), the field produced by the nanoparticle is effectively static during the 10 μ s lifetime of the radicals. There is no spin relaxation but $\Delta\Phi_s$ is changed because the field of the nanoparticle distorts the response of the radical pair to the direction of the geomagnetic field. Although not a relaxation effect, this could also prevent the compass from functioning. However, the impact of a static nanoparticle field is less pronounced than that of a nanoparticle that induces relaxation. Moreover, using a static field to disrupt the magnetoreceptor would potentially affect both a compass operating via the radical pair mechanism and one based on magnetite particles. For these reasons, we focus here on relaxation-inducing nanoparticles, as this method of disrupting the compass is selective for the radical pair mechanism. For intermediate τ_N , the relaxation is at its most efficient when 10 ns $< \tau_N < 1$ μ s. In this range, $\Delta\Phi_s \approx 0$ and the response of the radical pair to both the presence and direction of the geomagnetic field vanishes.

Figure 2(b) demonstrates that Brownian motion of the nanoparticle ($d = 12$ nm, $\Delta d = 2$ nm, figure 1) relaxes the radical pair much less efficiently than does the Néel fluctuation of the magnetic moment. For hopping times between 1 ps and 1 s, the relative motion of the nanoparticle and the radical pair gives rise to relatively little spin relaxation in the absence of Néel relaxation and hardly changes the spin dynamics in the presence of Néel relaxation. Since we wish the nanoparticle to be attached to cryptochrome to maximise the selectivity of the relaxation enhancement, its motion would have to be quite constrained. Consequently, as demonstrated in figure 2(b), the modulation of the field experienced by the radicals is likely to be much weaker than the full field-reversal arising from Néel fluctuations. From now on we therefore focus exclusively on the latter.

In summary, the nanoparticle must undergo Néel relaxation that is neither too slow nor too fast if it is to have the desired effect of efficiently relaxing the spins of a nearby radical pair. Ideally, τ_N should be in the range 10 ns–1 μ s.

3.2 Magnetic moment and position of the nanoparticle

To estimate the required magnitude of the magnetic moment of the nanoparticle and its distance from the radicals, we simulated a more realistic spin system based on the radicals responsible for the observed magnetic field effects on purified cryptochromes [11, 12]. Formed by photo-induced electron transfer within the protein, this radical pair comprises the reduced form of the non-covalently bound flavin adenine dinucleotide chromophore, $\text{FAD}^{\bullet-}$, and the oxidised form of a tryptophan amino acid residue, $\text{TrpH}^{\bullet+}$ [15]. The approach was the same as for the toy system above except that eight of the largest hyperfine interactions in the $[\text{FAD}^{\bullet-} \text{TrpH}^{\bullet+}]$ pair were included: N5, N10, H6 in the $\text{FAD}^{\bullet-}$ and N1, H1, H4, H7, H β in $\text{TrpH}^{\bullet+}$ (see Supplementary Information) [8, 9]. The primary radical, $\text{FAD}^{\bullet-}$, was oriented such that the short and long axes of the tricyclic isoalloxazine group defined the x- and y-axes, respectively. In this orientation, the dominant hyperfine interactions in $\text{FAD}^{\bullet-}$ (N5 and N10) are axially symmetric around the z-axis (as was the case for the toy system above). The secondary radical, $\text{TrpH}^{\bullet+}$, was rotated relative to $\text{FAD}^{\bullet-}$ as in the X-ray structure of *Drosophila melanogaster* cryptochrome [47, 48], and positioned on the x-axis 1.9 nm from the centre of the FAD.

Figure 3(a) shows the dependence of the singlet yield of the $[\text{FAD}^{\bullet-} \text{TrpH}^{\bullet+}]$ pair on the direction of a 50 μT magnetic field in the presence of periodically reversing local fields of strengths up to 400 μT directed along the x-axis. The Néel relaxation time was 1 ns (a typical value for magnetoferritin [50], see below) and the radical pair lifetime was 10 μs . As the field of the nanoparticle is increased, the “spike” at $\theta = 90^\circ$ is attenuated and $\Phi_s(\theta)$ tends towards the constant value (0.25) expected for fast relaxation. When the nanoparticle field exceeds 150 μT the spike is completely lost, which we take as a ‘sufficient’ alteration of the compass signal. If the radical pair lifetime is reduced from 10 μs to 1 μs , no spike is observed and ‘sufficient alteration’ is instead taken as the point at which more than 90% of the singlet yield anisotropy is lost. This occurs when the field produced by the nanoparticle exceeds 400 μT (see Supplementary Information).

Using a point dipole approximation and assuming that the nanoparticle is bound with its easy axis parallel to the x-axis of the radical pair, we can calculate how close a nanoparticle with a given magnetic moment would need to be to create a particular magnetic field at the mid-point of the two radicals. The results are shown in figure 3(b). For a magnetic moment of $350 \mu_B$, fields of 150 μT and 400 μT correspond to distances of 16.3 nm and 11.7 nm, respectively. If the magnetic moment is larger than $350 \mu_B$ or if the Néel relaxation is within the 10 ns–1 μs range identified above, then the nanoparticle could be placed further away.

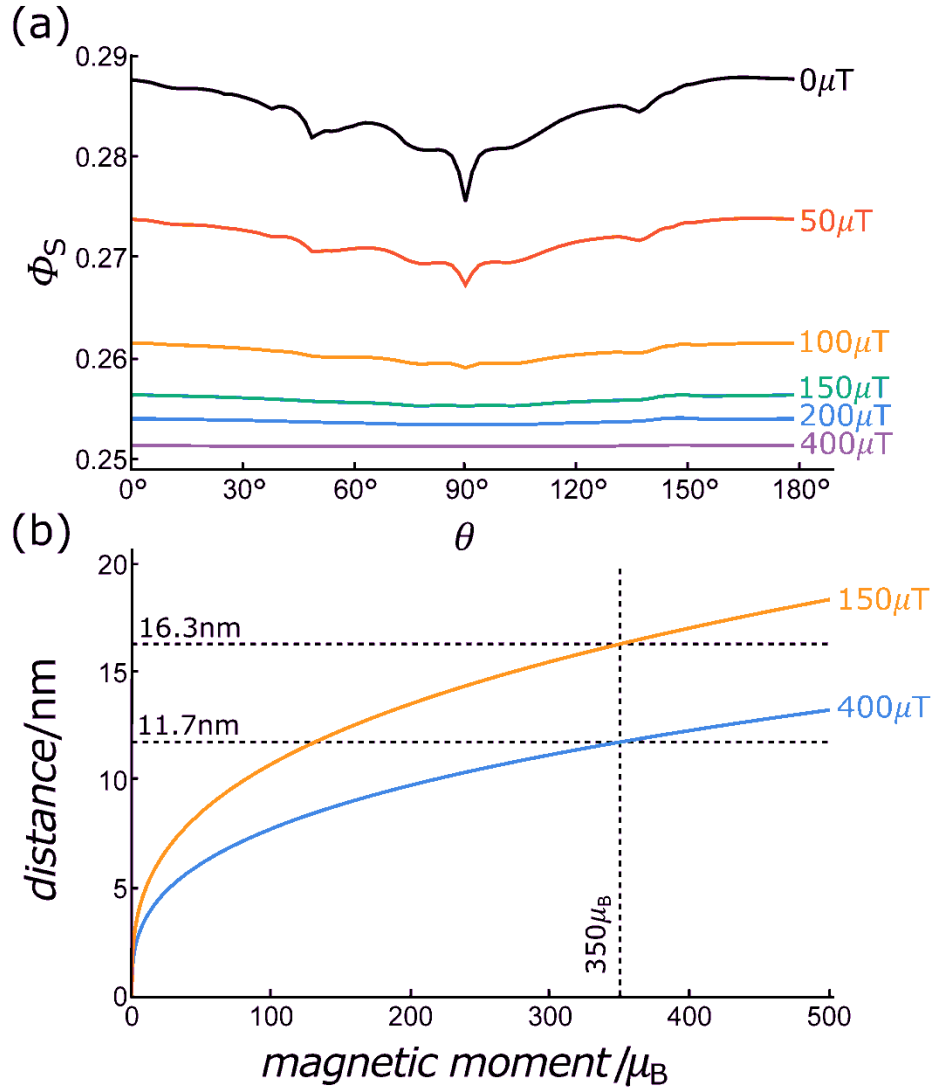


Figure 3. (a) The singlet yield, $\Phi_s(\theta)$, of the flavin-tryptophan radical pair in cryptochrome as a function of the direction of a 50 μT magnetic field, θ . The recombination lifetime of the radical pair was 10 μs . Both radicals were subjected to a periodically reversing local field in the range 0 to 400 μT . The mean time between field-reversals, τ_N , was 1 ns. (b) The distance from the centre of a nanoparticle at which the magnetic field it generates equals 150 μT or 400 μT as a function of its magnetic moment.

3.3 Choice of nanoparticle

The above considerations suggest that the key characteristics required for efficient relaxation of the electron spins of a $[\text{FAD}^{\bullet-} \text{TrpH}^{\bullet+}]$ radical pair are a superparamagnetic nanoparticle with a Néel relaxation time between 10 ns and 1 μs at a distance of roughly 12-16 nm. The chosen nanoparticle must, ultimately, be suitable for reproducible incorporation into a living system with the possibility of tailoring its properties. That is, it must be non-toxic and stable under physiological conditions with (ideally) uniform size and well-defined

magnetic properties. These are essentially the same requirements that must be met by MRI contrast agents, to which we looked for inspiration. Most magnetic nanoparticles that are used to enhance nuclear spin relaxation are based on either gadolinium (Gd^{3+}) chelates or superparamagnetic iron oxide [51]. They comprise three parts: a magnetic core, a biocompatible coating or shell, and a functionalized surface to target the particle to its intended substrate [51]. The coatings — commonly organic polymers, organic surfactants, or inorganic layers [37] — are particularly important for Gd^{3+} -based nanoparticles, which are otherwise highly toxic. An alternative approach, with clear advantages, is to use a protein cage to enclose the magnetic core. The biological origin of the cage imparts natural biocompatibility, minimises the toxicity of the mineral core, and makes the particles suitable for large-scale production [52]. Furthermore, the protein provides a versatile platform for functionalising the particle [53] and confines the growth of the core to produce uniformly sized particles.

The most commonly used protein template is ferritin — a class of spherical iron-storage proteins common to animals, plants and bacteria. Naturally occurring ferritin has an antiferromagnetically-ordered, single-domain, superparamagnetic ferrihydrite ($5\text{Fe}_2\text{O}_3 \cdot 9\text{H}_2\text{O}$) core, containing up to 4,500 Fe^{3+} ions [54], and around 2,000 on average [55]. Uncompensated iron spins at the surface of the core give ferritin an average magnetic moment of $300 \mu_B$ [56, 57]. It is water-soluble [58], resistant to denaturation, attracts high affinity antibodies, and is 12 nm in diameter, with an 8 nm internal cavity [59]. A further attractive feature of ferritin is that it is comparable in size to cryptochrome and so might not interfere excessively with its functioning *in vivo*. The same cannot be said of some of the other MRI nanoparticles, which can have hydrodynamic diameters of tens to hundreds of nanometres [51]. Furthermore, unlike many other nanoparticles, derivatives of human ferritin are capable of crossing a number of biological barriers, including the blood-brain barrier [38]. Bird retinæ are not vascularised but are provided with nutrients via the pecten. Observation of transferrin receptors binding ferritin in the retina [60] and of ferritin uptake from the bloodstream into the pecten [61] suggest that it may be able to enter the retina via this route.

The ability to synthesise cores with different magnetic properties inside an apo-ferritin shell offers the possibility of tailoring the nanoparticle to a particular application. In the present context, it would also allow one to devise a range of control experiments using empty (i.e. non-magnetic) apo-ferritin or a core whose magnetic properties are such that there should be no effect on a nearby radical pair sensor. Control experiments of this kind would confirm that any observed disruption to magnetic sensing arose from induced spin-relaxation rather than some non-magnetic effect on the structure or electron transfer ability of the cryptochrome.

There are many advantages to using the ferritin architecture to create a nanoparticle for the proposed experiment. Unfortunately, natural ferritin is not itself suitable: its Néel relaxation

time is less than 100 ps (table 1), which is too fast to relax a nearby radical pair (figure 2). However, the synthetic derivative magnetoferritin, in which the natural ferrihydrite core is replaced by magnetite (Fe_3O_4), has a Néel relaxation time of 1–5 ns. Although this lies outside the optimum range identified above, it should still drive reasonably fast relaxation. According to figure 3, if magnetoferritin were loaded so as to have a magnetic moment of $350 \mu_B$, which is well within the range of measured values (table 1), it would need to be bound with the centre of the nanoparticle approximately 12 nm from the radicals for them to experience a 400 μT field. Given the dimensions of cryptochrome (approximately $5 \times 6 \times 9$ nm [47, 48]) and the 6 nm radius of magnetoferritin, this appears feasible.

Table 1. Magnetic properties of ferritin and magnetoferritin.

	Ferritin ^a	Magnetoferritin ^{b,c}
magnetic moment	$300 \mu_B$	$4,636 \mu_B^c$ $13\text{--}350 \mu_B^b$
attempt frequency, f_0	$1 \times 10^{11} - 5 \times 10^{12} \text{ s}^{-1}$	10^9 s^{-1}^c
U / k_B^d	180–400 K	$98\text{--}197 \text{ K}^c$ $25\text{--}381 \text{ K}^b$
Néel relaxation time		
$\tau_N = \frac{1}{f_0} \exp\left(\frac{U}{k_B T}\right)$	$3.6 \times 10^{-13} - 3.6 \times 10^{-11} \text{ s}^e$	$1.1\text{--}3.4 \times 10^{-9} \text{ s}^e$

^a Ref. [57].

^b Ref. [49]

^c Ref. [50]

^d U here represents the height of the energy barrier separating different orientations of the nanoparticle's magnetic moment.

^e At 310 K.

3.4 Practical considerations

Clearly, there are challenges that would have to be faced before our proposal could be realised in behavioural tests on migratory songbirds, or even in more tractable model organisms such as *Drosophila*. In particular, delivering synthetic nanoparticles reliably and specifically to an unknown (but potentially large) number of intracellular cryptochromes may be beyond the reach of current technology. A more feasible option could be to devise a way to genetically engineer a magnetoferritin nanoparticle already attached via a flexible linker to cryptochrome. A literature search revealed no well-developed biosynthetic route to magnetoferritin, although there are suggestions that it might be possible to convert ferritin into magnetoferritin genetically. For example, a study by Matsumoto *et al.* describes a mutant form of ferritin from thermophilic bacteria, with approximately three times higher

iron uptake than normal human ferritin [62]. The higher iron uptake was associated with larger magnetic moments although the mineral composition of the mutated cores was not characterised. Increased iron uptake in malfunctioning human brain ferritin is associated with a number of neurodegenerative diseases and is thought to result in deposits of biogenic magnetite [63-65]. However, the protein shell of this pathological ferritin does not function correctly and allows large amounts of iron to pass out of the protein into the blood stream, where it can reach toxic levels [63]. Finally, biogenic magnetite has been reported to form at least part of the core of plant ferritin (phytoferritin) [66, 67].

An alternative to a behavioural approach would be to measure magnetic field effects on the neuronal firing of an explanted retina, which should provide a good measure of compass function [14]. It is likely to be easier to deliver nanoparticles to an isolated retina than to an intact bird, where magnetoferritin can be rapidly removed from the bloodstream by the liver [39]. Nanoparticles could even be injected directly into the cells thought to harbour the magnetic sensors. As an added advantage, the measured magnetic response would not rely on the bird's motivation to orient and would probably be less susceptible to any side-effects of the nanoparticles. In particular, the potential toxicity of high levels of magnetoferritin is unknown, although, as mentioned above, high levels of leakage of iron oxide out of the protein shell over longer periods of time are associated with various neurodegenerative diseases. High concentrations of nanoparticles would probably need to be injected into the animal or retina because the number of cryptochrome proteins per cell, the number that would need to be deactivated to observe a changed behavioural response and the success rate with which the nanoparticles bind are all unknown, making it difficult to reliably judge the quantity of nanoparticles that would be required. The risk associated with this would be reduced if the nanoparticles were delivered directly to the site of interest, allowing the experiment to have a shorter timescale.

3.5 Simulation of preliminary experiments

Before attempting *in vivo* experiments, whether on whole organisms or explanted retinas, the effect of magnetoferritin on cryptochrome would need to be verified *in vitro*. Most measurements of magnetic field effects on radical pair reactions have been made in solution where rapid rotational tumbling leads to efficient averaging of the anisotropic components of the hyperfine interactions. Such experiments cannot therefore provide information on the singlet yield anisotropy that forms the basis of the compass sensors discussed above. Instead, they typically measure the isotropic singlet yield Φ_s^{iso} as a function of the strength of the applied magnetic field. Experiments such as these could be used rather straightforwardly to investigate the efficiency with which an attached magnetoferritin particle relaxes the spins of a photo-induced radical pair in a purified cryptochrome molecule. If the presence of the magnetoferritin changes the field-dependence of Φ_s^{iso} by enhancing the electron spin relaxation, then it should also affect the

singlet yield anisotropy, $\Delta\Phi_s$, of the aligned, immobilized radical pairs that have been proposed as the compass sensors in the retina.

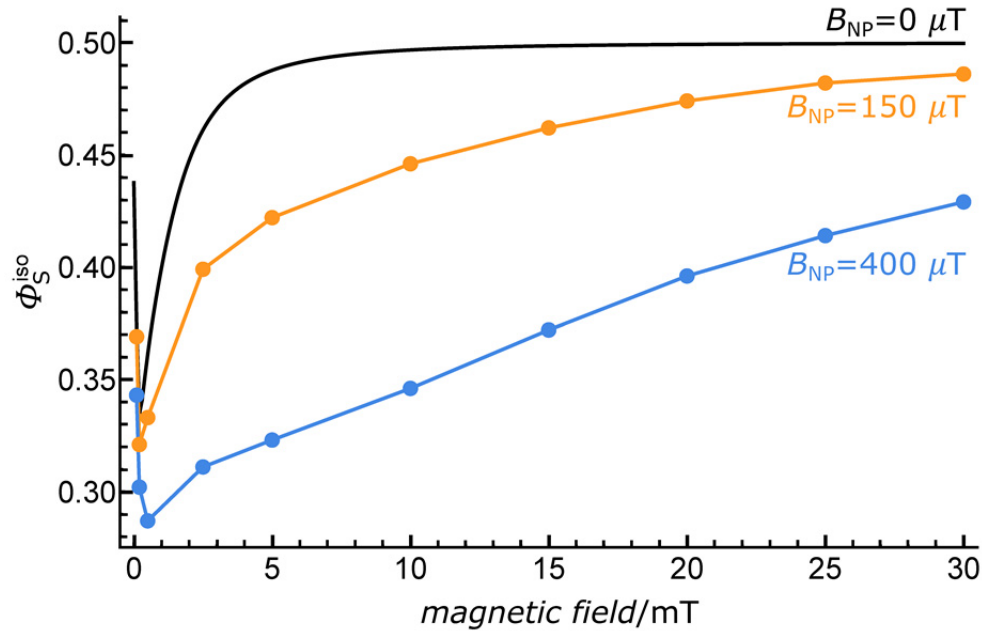


Figure 4. The singlet yield Φ_s^{iso} as a function of the strength of an applied magnetic field, B_0 , for a model flavin-tryptophan radical pair containing only the isotropic components of the hyperfine tensors. The presence of a nanoparticle created a 150 μT or 400 μT field at the radical pair (blue and orange lines, respectively). This field was averaged over 500 randomly chosen orientations of the nanoparticle. The solid black line is the singlet yield in the absence of a nanoparticle. For the averaged data, the singlet yield was only calculated at the marked points, due to the length of the calculation. The field of the nanoparticle was experienced equally by both radicals. The radical pair recombination lifetime was 1 μs and the Néel relaxation time of the nanoparticle was 1 ns.

Figure 4 shows simulated isotropic magnetic field effects (Φ_s^{iso} as a function of field strength) for the model cryptochrome radical pair used for figure 3(a), with the anisotropic components of the hyperfine tensors discarded. The recombination lifetime of the radical pair was 1 μs . Tethered to the radical pair is a magnetoferritin nanoparticle generating an instantaneous field of either 150 μT or 400 μT at both radicals. The Néel relaxation time of the nanoparticle was 1 ns. Φ_s^{iso} was averaged over 500 randomly chosen orientations of the nanoparticle field relative to the applied magnetic field. The isotropic nature of the hyperfine interactions means that neither the orientation of the nanoparticle field or of the applied magnetic field relative to the radical pair need be considered.

In the absence of the nanoparticle (figure 4, black line), the field-dependence of Φ_s^{iso} has a characteristic biphasic shape. For weak fields (≤ 1 mT), the singlet yield shows a sharp

decrease, known as the Low Field Effect, resulting from the increased efficiency of singlet-triplet interconversion caused by lifting the degeneracy of coherent spin states [46, 68]. At higher fields, the Zeeman interaction with the external field causes two of the three triplet sub-states to become energetically isolated, so reducing the extent of singlet-triplet mixing. The effect reaches a plateau when the applied field strength is significantly larger than the hyperfine interactions.

The fluctuating field from the nanoparticle induces spin relaxation, which reduces the singlet yield, and increases the field strength at which the plateau is reached (figure 4, blue and orange lines). Such broadening effects are characteristic of rapidly relaxing radical pairs and have been observed on many occasions [12, 69, 70]. Very similar effects are predicted (see Supplementary Information) when the field of the nanoparticle only relaxes one of the radicals.

The simulations shown in figure 4 are not expected to be a quantitative prediction of experimental results, particularly given that only a small number of hyperfine interactions were included in the cryptochrome model and all spin relaxation processes, apart from those induced by Néel relaxation, were ignored. However, the results indicate that magnetic field effects on a flavin-tryptophan radical pair should be measurably altered by the addition of a magnetoferritin nanoparticle attached to at least one of the radicals. Experimental verification of this effect would provide an essential test of the proposed *in vivo* experiment, and would allow the properties of the nanoparticle and length of the cryptochrome–nanoparticle linker to be optimized. Such studies would also allow the above-mentioned negative controls (apo-ferritin and ferritin itself) to be tested.

4. Conclusions

We have proposed here an experiment to test the role of cryptochrome in avian magnetoreception using superparamagnetic nanoparticles to disable its presumed magnetic sensing role. The principle is to use the fluctuating magnetic field arising from the Néel relaxation of the nanoparticle to induce efficient spin relaxation in the sensory radical pair and so destroy its ability to respond to the geomagnetic field. In principle, this would be an extremely gentle perturbation, involving molecular interactions many orders of magnitude smaller than $k_B T$. Using spin dynamics simulations, we have shown that the synthetic, protein-based nanoparticle, magnetoferritin has the required magnetic properties: its Néel relaxation time is within the required range and its instantaneous magnetic moment can be tailored to an appropriate value. We estimate that the centre of the nanoparticle would need to be about 12-16 nm away from the radicals to induce fast enough spin relaxation to disable the birds' magnetic compass in behavioural or electrophysiological experiments. The protein shell of magnetoferritin offers advantages in terms of biocompatibility, controlled synthesis and scope for control experiments. If this proposal can be implemented, we believe it has the power to distinguish between the two most likely functions of cryptochrome in magnetoreception — sensor and transducer. It could also be used to probe

the involvement of cryptochrome-based radical pairs in carcinogenic effects of extremely low frequency (e.g. 50 or 60 Hz) magnetic fields [71].

Data accessibility. This article has no additional data.

Authors' contributions. S.W. performed the study. S.W. and P.J.H. conceived and designed the study, discussed the results, and wrote the manuscript.

Competing interests. We declare we have no competing interests.

Funding. This work was supported by the European Research Council (under the European Union's 7th Framework Programme, FP7/2007-2013/ERC grant agreement no. 340451), the Air Force Office of Scientific Research (Air Force Materiel Command, USAF award no. FA9550-14-1-0095), and the Electromagnetic Fields Biological Research Trust.

Acknowledgements. We are grateful to Christiane Timmel, Stuart Mackenzie and Henrik Mouritsen for stimulating discussions during the course of this work.

Bibliography

1. Wiltschko, W., Merkel, F.W. 1966 Orientierung zugunruhiger Rotkehlchen im statischen Magnetfeld. *Verh. der Deutsch. Zoolog. Ges.* **59**, 362-367.
2. Wiltschko, W. 1968 Über den Einfluß statischer Magnetfelder auf die Zugorientierung der Rotkehlchen (*Erithacus rubecula*). *Z. Tierpsychol.* **25**, 537-558.
3. Nordmann, G.C., Hochstoeger, T., Keays, D.A. 2017 Magnetoreception - a sense without a receptor. *PLoS Biol.* **15**, e2003234.
4. Mouritsen, H. 2018 Long-distance navigation and magnetoreception in migratory animals. *Nature* **558**, 50-59.
5. Schulten, K., Swenberg, C.E., Weller, A. 1978 A biomagnetic sensory mechanism based on magnetic field modulated coherent electron spin motion. *Z. Phys. Chem. NF* **111**, 1-5.
6. Ritz, T., Adem, S., Schulten, K. 2000 A model for photoreceptor-based magnetoreception in birds. *Biophys. J.* **78**, 707-718.
7. Cintolesi, F., Ritz, T., Kay, C.W.M., Timmel, C.R., Hore, P.J. 2003 Anisotropic recombination of an immobilized photoinduced radical pair in a 50- μ T magnetic field: a model avian photomagnetoreceptor. *Chem. Phys.* **294**, 385-399.
8. Lee, A.A., Lau, J.C.S., Hogben, H.J., Biskup, T., Kattnig, D.R., Hore, P.J. 2014 Alternative radical pairs for cryptochrome-based magnetoreception. *J. Roy. Soc. Interface* **11**, 20131063.
9. Hiscock, H.G., Worster, S., Kattnig, D.R., Steers, C., Jin, Y., Manolopoulos, D.E., Mouritsen, H., Hore, P.J. 2016 The quantum needle of the avian magnetic compass. *Proc. Natl. Acad. Sci. USA* **113**, 4634-4639.
10. Liedvogel, M., Maeda, K., Henbest, K., Schleicher, E., Simon, T., Hore, P.J., Timmel, C.R., Mouritsen, H. 2007 Chemical magnetoreception: bird cryptochrome 1a is excited by blue light and forms long-lived radical-pairs. *Plos One* **2**, e1106.
11. Sheppard, D.M.W., Li, J., Henbest, K.B., Neil, S.R.T., Maeda, K., Storey, J., Schleicher, E., Biskup, T., Rodriguez, R., Weber, S., et al. 2017 Millitesla magnetic field effects on the photocycle of *Drosophila melanogaster* cryptochrome. *Sci. Rep.* **7**, 42228.
12. Maeda, K., Robinson, A.J., Henbest, K.B., Hogben, H.J., Biskup, T., Ahmad, M., Schleicher, E., Weber, S., Timmel, C.R., Hore, P.J. 2012 Magnetically sensitive light-induced reactions in cryptochrome are consistent with its proposed role as a magnetoreceptor. *Proc. Natl. Acad. Sci. USA* **109**, 4774-4779.
13. Liedvogel, M., Mouritsen, H. 2010 Cryptochromes—a potential magnetoreceptor: what do we know and what do we want to know? *J. Roy. Soc. Interface* **7**, S147-S162.

14. Mouritsen, H., Hore, P.J. 2012 The magnetic retina: light-dependent and trigeminal magnetoreception in migratory birds. *Curr. Opin. Neurobiol.* **22**, 343-352.
15. Hore, P.J., Mouritsen, H. 2016 The radical pair mechanism of magnetoreception. *Annu. Rev. Biophys.* **45**, 299-344.
16. Mouritsen, H., Janssen-Bienhold, U., Liedvogel, M., Feenders, G., Stalleicken, J., Dirks, P., Weiler, R. 2004 Cryptochromes and neuronal-activity markers colocalize in the retina of migratory birds during magnetic orientation. *Proc. Natl. Acad. Sci. USA* **101**, 14294-14299.
17. Niessner, C., Denzau, S., Gross, J.C., Peichl, L., Bischof, H.J., Fleissner, G., Wiltschko, W., Wiltschko, R. 2011 Avian ultraviolet/violet cones identified as probable magnetoreceptors. *Plos One* **6**, e20091.
18. Niessner, C., Gross, J.C., Denzau, S., Peichl, L., Fleissner, G., Wiltschko, W., Wiltschko, R. 2016 Seasonally changing cryptochrome 1b expression in the retinal ganglion cells of a migrating passerine bird. *Plos One* **11**, e0150377.
19. Bolte, P., Bleibaum, F., Einwich, A., Günther, A., Liedvogel, M., Heyers, D., Depping, A., Wöhlbrand, L., Rabus, R., Janssen-Bienhold, U., et al. 2016 Localisation of the putative magnetoreceptive protein cryptochrome 1b in the retinæ of migratory birds and homing pigeons. *Plos One* **11**, e0147819.
20. Günther, A., Einwich, A., Sjulstok, E., Feederle, R., Bolte, P., Koch, K.W., Solov'yov, A.V., Mouritsen, H. 2018 Double-cone localization and seasonal expression pattern suggest a role in magnetoreception for European robin cryptochrome 4. *Curr. Biol.* **28**, 211-223.
21. Gegebar, R.J., Casselman, A., Waddell, S., Reppert, S.M. 2008 Cryptochrome mediates light-dependent magnetosensitivity in *Drosophila*. *Nature* **454**, 1014-1018.
22. Gegebar, R.J., Foley, L.E., Casselman, A., Reppert, S.M. 2010 Animal cryptochromes mediate magnetoreception by an unconventional photochemical mechanism. *Nature* **463**, 804-807.
23. Foley, L.E., Gegebar, R.J., Reppert, S.M. 2011 Human cryptochrome exhibits light-dependent magnetosensitivity. *Nat Commun* **2**, 356.
24. Fedele, G., Edwards, M.D., Bhutani, S., Hares, J.M., Murbach, M., Green, E.W., Dissel, S., Hastings, M.H., Rosato, E., Kyriacou, C.P. 2014 Genetic analysis of circadian responses to low frequency electromagnetic fields in *Drosophila melanogaster*. *PLoS Genet.* **10**, e1004804.
25. Fedele, G., Green, E.W., Rosato, E., Kyriacou, C.P. 2014 An electromagnetic field disrupts negative geotaxis in *Drosophila* via a CRY-dependent pathway. *Nat. Commun.* **5**, 4391.
26. Yoshii, T., Ahmad, M., Helfrich-Forster, C. 2009 Cryptochrome mediates light-dependent magnetosensitivity of *Drosophila*'s circadian clock. *PLoS Biol.* **7**, 813-819.

27. Giachello, C.N.G., Scrutton, N.S., Jones, A.R., Baines, R.A. 2016 Magnetic fields modulate blue-light-dependent regulation of neuronal firing by cryptochrome. *J. Neurosci.* **36**, 10742-10749.
28. Marley, R., Giachello, C.N.G., Scrutton, N.S., Baines, R.A., Jones, A.R. 2014 Cryptochrome-dependent magnetic field effect on seizure response in *Drosophila* larvae. *Sci. Rep.* **4**, 5799.
29. Bazalova, O., Kvalicov, M., Valkova, T., Slaby, P., Bartos, P., Netusil, R., Tomanova, K., Braeunig, P., Lee, H.-J., Sauman, I., et al. 2016 Cryptochrome 2 mediates directional magnetoreception in cockroaches. *Proc. Natl. Acad. Sci. USA* **113**, 1660-1665.
30. Biskup, T., Hitomi, K., Getzoff, E.D., Krapf, S., Koslowski, T., Schleicher, E., Weber, S. 2011 Unexpected electron transfer in cryptochrome identified by time-resolved EPR spectroscopy. *Angew. Chem. Internat. Ed.* **50**, 12647-12651.
31. Biskup, T., Paulus, B., Okafuji, A., Hitomi, K., Getzoff, E.D., Weber, S., Schleicher, E. 2013 Variable electron transfer pathways in an amphibian cryptochrome tryptophan versus tyrosine-based radical pairs. *J. Biol. Chem.* **288**, 9249-9260.
32. Weber, S., Biskup, T., Okafuji, A., Marino, A.R., Berthold, T., Link, G., Hitomi, K., Getzoff, E.D., Schleicher, E., Norris, J.R. 2010 Origin of light-induced spin-correlated radical pairs in cryptochrome. *J. Phys. Chem. B* **114**, 14745-14754.
33. Rodgers, C.T., Hore, P.J. 2009 Chemical magnetoreception in birds: a radical pair mechanism. *Proc. Natl. Acad. Sci. USA* **106**, 353-360.
34. Kattnig, D.R., Solov'yov, I.A., Hore, P.J. 2016 Electron spin relaxation in cryptochrome-based magnetoreception. *Phys. Chem. Chem. Phys.* **18**, 12443-12456.
35. Kattnig, D.R., Sowa, J.K., Solov'yov, I.A., Hore, P.J. 2016 Electron spin relaxation can enhance the performance of a cryptochrome-based magnetic compass sensor. *New J. Phys.* **18**, 063007.
36. Worster, S., Kattnig, D.R., Hore, P.J. 2016 Spin relaxation of radicals in cryptochrome and its role in avian magnetoreception. *J. Chem. Phys.* **145**, 035104.
37. Issa, B., Obaidat, I.M., Albiss, B.A., Haik, Y. 2013 Magnetic nanoparticles: surface effects and properties related to biomedicine applications. *Int. J. Molec. Sci.* **14**, 21266-21305.
38. Cao, C.Q., Wang, X.X., Cai, Y., Sun, L., Tian, L.X., Wu, H., He, X.Q., Lei, H., Liu, W.F., Chen, G.J., et al. 2014 Targeted *in vivo* imaging of microscopic tumors with ferritin- based nanoprobes across biological barriers. *Adv. Mater.* **26**, 2566-2571.
39. Bulte, J.W.M., Kraitchman, D.L. 2004 Iron oxide MR contrast agents for molecular and cellular imaging. *NMR Biomed.* **17**, 484-499.

40. Cohen, A.E. 2009 Nanomagnetic control of intersystem crossing. *J. Phys. Chem. A* **113**, 11084-11092.
41. Cai, J. 2011 Quantum probe and design for a chemical compass with magnetic nanostructures. *Phys. Rev. Lett.* **106**, 100501.
42. Binhi, V. 2008 Do naturally occurring magnetic nanoparticles in the human body mediate increased risk of childhood leukaemia with EMF exposure? *Int. J. Radiat. Biol.* **84**, 569-579.
43. Kavokin, K. 2017 Can a hybrid chemical-ferromagnetic model of the avian compass explain its outstanding sensitivity to magnetic noise? *Plos One* **12**, e0173887.
44. Meister, M. 2016 Physical limits to magnetogenetics. *Elife* **5**, e17210.
45. Worster, S. 2018 Order, motion and relaxation in radical pair compass magnetoreception, D.Phil. thesis, University of Oxford.
46. Timmel, C.R., Till, U., Brocklehurst, B., McLauchlan, K.A., Hore, P.J. 1998 Effects of weak magnetic fields on free radical recombination reactions. *Molec. Phys.* **95**, 71-89.
47. Levy, C., Zoltowski, B.D., Jones, A.R., Vaidya, A.T., Top, D., Widom, J., Young, M.W., Scrutton, N.S., Crane, B.R., Leys, D. 2013 Updated structure of *Drosophila* cryptochrome. *Nature* **495**, E3-E4.
48. Zoltowski, B.D., Vaidya, A.T., Top, D., Widom, J., Young, M.W., Crane, B.R. 2011 Structure of full-length *Drosophila* cryptochrome. *Nature* **480**, 396-399.
49. Martinez-Perez, M.J., de Miguel, R., Carbonera, C., Martinez-Julvez, M., Lostao, A., Piquer, C., Gomez-Moreno, C., Bartolome, J., Luis, F. 2010 Size-dependent properties of magnetoferritin. *Nanotechnology* **21**, 465707.
50. Moskowitz, B.M., Frankel, R.B., Walton, S.A., Dickson, D.P.E., Wong, K.K.W., Douglas, T., Mann, S. 1997 Determination of the preexponential frequency factor for superparamagnetic maghemite particles in magnetoferritin. *J. Geophys. Res.* **102**, 22671-22680.
51. Na, H.B., Song, I.C., Hyeon, T. 2009 Inorganic nanoparticles for MRI contrast agents. *Adv. Mater.* **21**, 2133-2148.
52. Klem, M.T., Young, M., Douglas, T. 2005 Biomimetic magnetic nanoparticles. *Mater. Today* **8**, 28-37.
53. Uchida, M., Flenniken, M.L., Allen, M., Willits, D.A., Crowley, B.E., Brumfield, S., Willis, A.F., Jackiw, L., Jutila, M., Young, M.J., et al. 2006 Targeting of cancer cells with ferrimagnetic ferritin cage nanoparticles. *J. Am. Chem. Soc.* **128**, 16626-16633.
54. Harrison, P.M., Arosio, P. 1996 Ferritins: molecular properties, iron storage function and cellular regulation. *Biochim. Biophys. Acta* **1275**, 161-203.

55. Harris, J.G.E., Grimaldi, J.E., Awschalom, D.D., Chiolero, A., Loss, D. 1999 Excess spin and the dynamics of antiferromagnetic ferritin. *Phys. Rev. B* **60**, 3453-3456.
56. Kilcoyne, S.H., Cywinski, R. 1995 Ferritin - a model superparamagnet. *J. Magn. Magn. Mater.* **140**, 1466-1467.
57. Vohralik, P.F., Lam, S.K.H. 2009 NanoSQUID detection of magnetization from ferritin nanoparticles. *Supercon. Sci. Technol.* **22**, 64007.
58. Allen, P.D., St Pierre, T.G., Chua-anusorn, W., Strom, V., Rao, K.V. 2000 Low-frequency low-field magnetic susceptibility of ferritin and hemosiderin. *Biochim. Biophys. Acta* **1500**, 186-196.
59. Arosio, P., Ingrassia, R., Cavadini, P. 2009 Ferritins: a family of molecules for iron storage, antioxidation and more. *Biochim. Biophys. Acta* **1790**, 589-599.
60. Cho, S.S., Lucas, J.J., Hyndman, A.G. 1999 Transferrin binding protein is expressed by oligodendrocytes in the avian retina. *Brain Res.* **816**, 229-233.
61. Seaman, A.R. 1966 Ultrafine architecture of the avian "pecten oculi". *Albrecht v. Graefes Arch. Klin. Exp. Ophthalm.* **170**, 1-15.
62. Matsumoto, Y., Chen, R., Anikeeva, P., Jasanoff, A. 2015 Engineering intracellular biomineralization and biosensing by a magnetic protein. *Nat Commun* **6**, 8721.
63. Quintana, C., Cowley, J.M., Marhic, C. 2004 Electron nanodiffraction and high-resolution electron microscopy studies of the structure and composition of physiological and pathological ferritin. *Journal of Structural Biology* **147**, 166-178.
64. Gossuin, Y., Hautot, D., Muller, R.N., Pankhurst, Q., Dobson, J., Morris, C., Gillis, P., Collingwood, J. 2005 Looking for biogenic magnetite in brain ferritin using NMR relaxometry. *NMR Biomed.* **18**, 469-472.
65. Koralewski, M., Klos, J.W., Baranowski, M., Mitroova, Z., Kopcansky, P., Melnikova, L., Okuda, M., Schwarzscher, A. 2012 The Faraday effect of natural and artificial ferritins. *Nanotechnology* **23**, 355704.
66. Gajdardziska-Josifovska, M., McClean, R.G., Schofield, M.A., Sommer, C.V., Kean, W.F. 2001 Discovery of nanocrystalline botanical magnetite. *Eur. J. Mineral.* **13**, 863-870.
67. Stormer, F.C., Wielgolaski, F.E. 2010 Are magnetite and ferritin involved in plant memory? *Rev. Environ. Sci. Biotechnol.* **9**, 105-107.
68. Brocklehurst, B. 1976 Spin correlation in geminate recombination of radical ions in hydrocarbons. 1. Theory of magnetic-field effect. *J. Chem. Soc. Faraday Trans. II* **72**, 1869-1884.

69. Miura, T., Maeda, K., Arai, T. 2006 The spin mixing process of a radical pair in low magnetic field observed by transient absorption detected nanosecond pulsed magnetic field effect. *J. Phys. Chem. A* **110**, 4151-4156.
70. Zollitsch, T.M., Jarocho, L.E., Bialas, C., Henbest, K.B., Kodali, G., Dutton, P.L., Moser, C.C., Timmel, C.R., Hore, P.J., Mackenzie, S.A. 2018 Magnetically sensitive radical photochemistry of non-natural flavoproteins. *J. Am. Chem. Soc.* **140**, 8705-8713.
71. Juutilainen, J., Herrala, M., Luukkonen, J., Naarala, J., Hore, P.J. 2018 Magnetocarcinogenesis: is there a mechanism for carcinogenic effects of weak magnetic fields? *Proc. R. Soc. B* **285**, 20180590.

Proposal to use superparamagnetic nanoparticles to test the role of cryptochrome in magnetoreception

Susannah Bourne Worster and P. J. Hore*

Department of Chemistry, University of Oxford, Physical and Theoretical Chemistry Laboratory,
South Parks Road, Oxford OX1 3QZ, U.K.

* Author for correspondence: peter.hore@chem.ox.ac.uk

Electronic Supplementary Material

	Page
S1. Calculation of the singlet yield	2
S2. A four-site model of Brownian motion and Néel relaxation	4
S3. Effect of the orientation of the nanoparticle easy axis on relaxation in a realistic radical pair	5
S4. Hyperfine interactions of FAD ^{•−} and TrpH ^{•+}	6
S5. Required nanoparticle field strength to deactivate a short-lived radical pair compass	8
S6. Orientation sampling	9
S7. Simulations of an intermolecular radical pair reaction <i>in vitro</i>	10
References	11

S1. Calculation of the singlet yield

The fractional yield of singlet product can be calculated using a simple rate equation to describe the reaction of the radical pair from its singlet state:

$$\Phi_s = \Phi_s(\infty) = \int_0^\infty k_s[S(t)]dt = k \int_0^\infty P_s(t) \exp(-kt)dt,$$

where $P_s(t)$ is the probability that the radical pair is in its singlet state in the absence of recombination reactions and $[S(t)]$ is the normalized ($[S(0)] = 1$) concentration of singlet radical pairs present at time t during the reaction. It is assumed that the singlet and triplet radical pairs are both removed at the same rate by first-order reactions with rate constants $k_s = k_t = k$.

The probability of a radical pair existing in the singlet state is calculated by taking the trace of the density matrix $\hat{\rho}(t)$ with the singlet projection operator \hat{P}^s :

$$P_s(t) = \text{Tr}[\hat{\rho}(t)\hat{P}^s].$$

The evolution of the density matrix is captured by the Liouville-von Neumann equation

$$\frac{d\hat{\rho}(t)}{dt} = -\hat{L}\hat{\rho}(t).$$

In the two-site model used in the main text, the Liouville superoperator \hat{L} is constructed from the Liouville superoperators corresponding to each site and the rate constants for transitions between the two sites (see equation (2.1) in the main text). The single site Liouville superoperators (equation 2.2 in the main text) contain the interactions of the two unpaired electrons with the Earth's magnetic field and with any magnetic nuclei in the radicals,

$$\hat{H}_0 = \gamma_e B_0 \left[(S_z^{(1)} + S_z^{(2)}) \cos \theta + (S_x^{(1)} + S_x^{(2)}) \sin \theta \cos \phi + (S_y^{(1)} + S_y^{(2)}) \sin \theta \sin \phi \right] + \sum_{i=1,2} \sum_n \mathbf{I}_n \cdot \mathbf{A}_{n,i} \cdot \mathbf{S}^{(i)},$$

as well as with the magnetic field produced by the nanoparticle,

$$\hat{H}_{A/B} = \gamma_e \left[B_N(\mathbf{r}_{A/B}^{(1)}) \cdot \mathbf{S}^{(1)} + B_N(\mathbf{r}_{A/B}^{(2)}) \cdot \mathbf{S}^{(2)} \right].$$

The operators $\mathbf{S}^{(i)}$ and \mathbf{I}_n represent, respectively, the spins of the two electrons and any magnetic nuclei, $\mathbf{A}_{n,i}$ is a tensor describing the hyperfine interaction between one unpaired electron and one magnetic nucleus; γ_e is the gyromagnetic ratio of an electron; B_0 is the Earth's field strength and θ and ϕ are polar and azimuthal angles describing the direction of the Earth's field relative to the principal axis of the hyperfine interactions in the radical pair. The nanoparticle is modelled as a point dipole that produces a field at position \mathbf{r}

$$B_n(\mathbf{r}) = \frac{\mu_0}{4\pi} \left(\frac{3(\mathbf{m} \cdot \mathbf{r})\mathbf{r}}{r^5} - \frac{\mathbf{m}}{r^3} \right),$$

where \mathbf{m} is the instantaneous magnetic moment of the particle.

For larger spin systems, the size of the calculation was reduced by first exchanging the top and bottom rows of the linear system

$$\hat{L} \begin{pmatrix} x_u \\ x_l \end{pmatrix} = \begin{pmatrix} \hat{\rho}(0) \\ \hat{\rho}(0) \end{pmatrix},$$

then carrying out the first step of a Gaussian elimination to give

$$\begin{pmatrix} -\frac{\hat{1}}{\tau_N} & \left(\hat{L}_2 + \frac{\hat{1}}{\tau_N} \right) \\ 0 & -\frac{\hat{1}}{\tau_N} + \left(\hat{L}_1 + \frac{\hat{1}}{\tau_N} \right) \tau_N \left(\hat{L}_2 + \frac{\hat{1}}{\tau_N} \right) \end{pmatrix} \begin{pmatrix} x_u \\ x_l \end{pmatrix} = \begin{pmatrix} \hat{\rho}(0) \\ \hat{\rho}(0) + \left(\hat{L}_1 + \frac{\hat{1}}{\tau_N} \right) \tau_N \hat{\rho}(0) \end{pmatrix}.$$

The lower line of the transformed linear system was solved first, using the BICGSTAB solver with an initial guess of

$$x = \left(\left(\hat{L}_1 + \frac{\hat{1}}{\tau_N} \right) \tau_N \left(\hat{L}_2 + \frac{\hat{1}}{\tau_N} \right) \right)^{-1} \left(\hat{\rho}(0) + \left(\hat{L}_1 + \frac{\hat{1}}{\tau_N} \right) \tau_N \hat{\rho}(0) \right).$$

It was assumed that the radical pair was formed in a pure singlet state, such that

$$\begin{pmatrix} \hat{\rho}(0) \\ \hat{\rho}(0) \end{pmatrix} = \frac{1}{Z} \begin{pmatrix} \hat{\rho}^s \\ \hat{\rho}^s \end{pmatrix}.$$

S2. A four-site model of Brownian motion and Néel relaxation

The main text introduces a two-site model to describe Néel relaxation or Brownian motion of the nanoparticle (a very approximate description in the case of Brownian motion). To generate the results in figure 2(b), the model was extended to four sites:

$$\frac{d}{dt} \begin{pmatrix} \hat{\rho}_1 \\ \hat{\rho}_2 \\ \hat{\rho}_3 \\ \hat{\rho}_4 \end{pmatrix} = \begin{pmatrix} -\hat{L}_1 - \hat{1}/\tau_N - k_B \hat{1} & \hat{1}/\tau_N & k_B \hat{1} & 0 \\ \hat{1}/\tau_N & -\hat{L}_2 - \hat{1}/\tau_N - k_B \hat{1} & 0 & k_B \hat{1} \\ k_B \hat{1} & 0 & -\hat{L}_3 - \hat{1}/\tau_N - k_B \hat{1} & \hat{1}/\tau_N \\ 0 & k_B \hat{1} & \hat{1}/\tau_N & -\hat{L}_4 - \hat{1}/\tau_N - k_B \hat{1} \end{pmatrix} \begin{pmatrix} \hat{\rho}_1(t) \\ \hat{\rho}_2(t) \\ \hat{\rho}_3(t) \\ \hat{\rho}_4(t) \end{pmatrix}.$$

Sites 1 and 2 have the nanoparticle and the radicals in the same positions but opposing orientations of the magnetic moment of the nanoparticle. The same is true for sites 3 and 4. In other words, these two pairs of sites each form a copy of the original two-site model of Néel relaxation. Sites 1 and 3 differ in the distance of the nanoparticle from the radicals, as do sites 2 and 4. This creates a two-site model for nanoparticle ‘hopping’, where k_B is the rate constant for the Brownian hopping. In each site, the magnetic field from the nanoparticle at the radical pair is calculated using the point-dipole approximation. Note that Z in the expression for $\Phi_s(\theta)$ corresponding to equation (2.3), the number of nuclear spin states, will now be four times its value for a single site.

The extension to a four-site model allows the effects of Néel relaxation and Brownian motion to be investigated concurrently. However, the two mechanisms are prevented from interacting with each other – the nanoparticle never simultaneously changes its position and the orientation of its magnetic moment.

S3. Effect of the orientation of the nanoparticle easy axis on relaxation in a realistic radical pair

Figure S1 illustrates that, for a more complex radical pair, any orientation of the nanoparticle easy axis will induce relaxation (in contrast to the case of the simplified model radical pair used in figure 2(a) of the main text). However, the most efficient relaxation still occurs when the easy axis of the nanoparticle is perpendicular to the dominant hyperfine interactions in the radical pair.

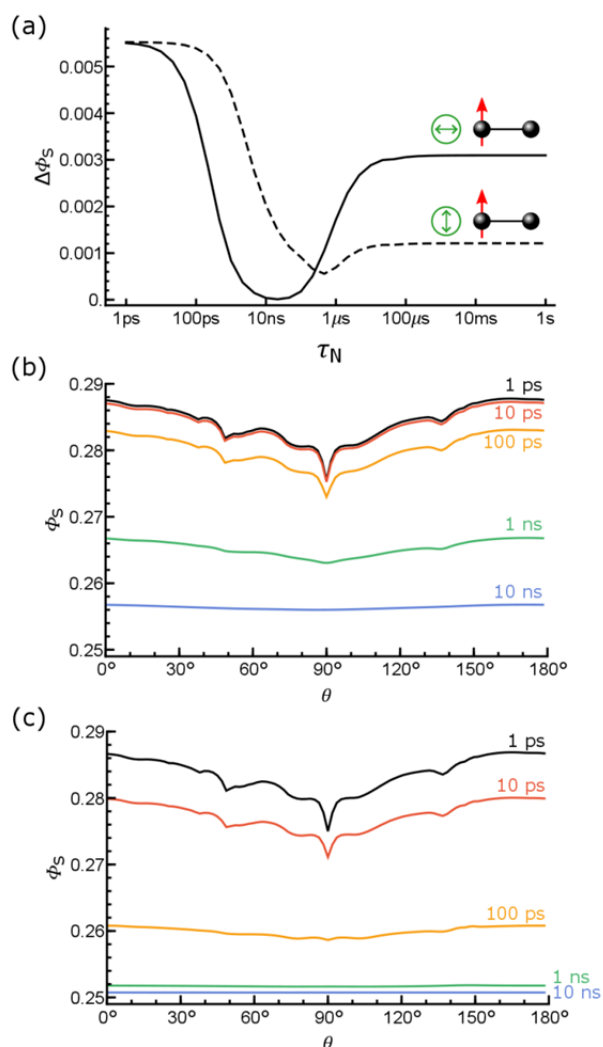


Figure S1. (a) The dependence of the singlet yield anisotropy, $\Delta\Phi_S$, on the Néel relaxation time (τ_N) for the 10-spin model of the flavin-tryptophan radical pair in cryptochrome (see main text). The radical pair recombination lifetime $\tau = 1 \mu s$. (b) and (c) show similar data for $\tau = 10 \mu s$. The nanoparticle is situated at -12 nm along the inter-radical axis, which has its origin at the flavin radical. Its easy axis lies either parallel (dotted lines and (b)) or perpendicular (solid lines and (c)) to the principal axis of the large N5 hyperfine interaction in the flavin radical. The strength of the external (Earth's) field is $50 \mu T$.

S4. Hyperfine interactions of FAD^{•-} and TrpH^{•+}

In this work a 10-spin (8-nuclear) model of the flavin-tryptophan radical pair in cryptochrome is used. The 8 nuclei, listed in the tables below, were chosen from among those with the largest hyperfine couplings based on previous studies that showed they had the largest impact on both the shape of the compass signal and the relaxation behaviour of the radical pair [1,2].

Table S1. Hyperfine tensors for the FAD^{•-} radical. Calculated using density functional theory in Gaussian-03 (1) at the UB3LYP/EPR-III level.[♥]

Nucleus	A	$a_{\text{iso}}/\text{mT}^\diamond$	$T_{\text{qq}}/\text{mT}^*$
N5	$\begin{pmatrix} -0.0925 & 0.0029 & 0.0 \\ 0.0029 & -0.0875 & 0.0 \\ 0.0 & 0.0 & 1.7569 \end{pmatrix}$	0.5233	1.2336
			-0.6101
			-0.6234
N10	$\begin{pmatrix} -0.0149 & -0.0021 & 0.0 \\ -0.0021 & -0.0237 & 0.0 \\ 0.0 & 0.0 & 0.6046 \end{pmatrix}$	0.1887	0.4159
			-0.2031
			-0.2128
H6	$\begin{pmatrix} -0.2009 & -0.0328 & 0.0 \\ -0.0328 & -0.5271 & 0.0 \\ 0.0 & 0.0 & -0.4336 \end{pmatrix}$	-0.3872	0.1896
			-0.0464
			-0.1432

[♥]Calculated by Dr Ilya Kuprov, Department of Chemistry, University of Southampton [3]. The calculation was done for the radical anion of 7,8,10-trimethyl isoalloxazine (lumiflavin) *in vacuo*. The atom numbering scheme is shown below.

[♦]Isotropic hyperfine interactions.

^{*}Principal anisotropic components of the hyperfine tensors (arranged in descending order of magnitude for each nucleus).

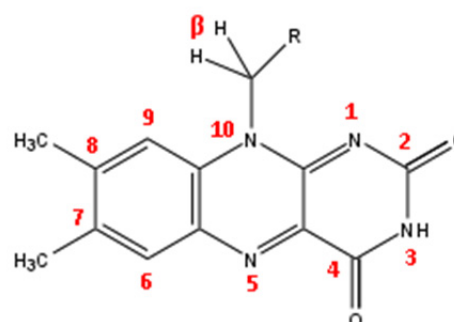


Table S2. Hyperfine tensors for the TrpH^{•+} radical. Calculated using density functional theory in Gaussian-03 (1) at the UB3LYP/EPR-III level.[♥]

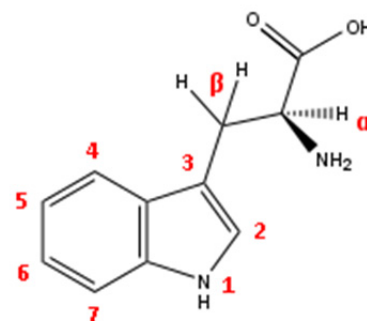
Nucleus	A [^]	a_{iso}/mT [♦]	T_{qq}/mT [*]
N1	$\begin{pmatrix} -0.0336 & 0.0924 & -0.1354 \\ 0.0924 & 0.3303 & -0.5318 \\ -0.1354 & -0.5318 & 0.6680 \end{pmatrix}$	0.3215	0.7596 -0.3745 -0.3851
H1	$\begin{pmatrix} -0.9920 & -0.2091 & -0.2003 \\ -0.2091 & -0.2631 & 0.2803 \\ -0.2003 & 0.2803 & -0.5398 \end{pmatrix}$	-0.5983	0.5914 -0.1071 -0.4843
H4	$\begin{pmatrix} -0.5596 & -0.1956 & -0.1657 \\ -0.1956 & -0.4020 & 0.0762 \\ -0.1657 & 0.0762 & -0.5021 \end{pmatrix}$	-0.4880	0.3001 -0.0480 -0.2520
H7	$\begin{pmatrix} -0.4355 & -0.1541 & -0.1239 \\ -0.1541 & -0.2777 & 0.0864 \\ -0.1239 & 0.0864 & -0.377 \end{pmatrix}$	-0.3636	0.2540 -0.0594 -0.1945
Hβ1	$\begin{pmatrix} 1.5808 & -0.0453 & -0.0506 \\ -0.0453 & 1.5575 & 0.0988 \\ -0.0506 & 0.0988 & 1.6752 \end{pmatrix}$	1.6046	0.1521 -0.0456 -0.1065

[♥]Calculated by Dr Ilya Kuprov, Department of Chemistry, University of Southampton [3]. The calculation was done for the radical cation of tryptophan *in vacuo*. The atom numbering scheme is shown below.

[^]Full hyperfine tensors in the same axis system as FAD^{•+} (Table S1). The relative orientation of the two radicals was taken to be that of the FAD cofactor and Trp-342 (the terminal tryptophan of the Trp-triad) in the crystal structure of *Drosophila melanogaster* cryptochrome (DmCry, PDB entry 4GU5 [4,5]).

[♦]Isotropic hyperfine interactions.

^{*}Principal anisotropic components of the hyperfine tensors (arranged in descending order of magnitude for each nucleus).



S5. Required nanoparticle field strength to deactivate a short-lived radical pair compass

Figure 3 in the main text illustrates the loss of singlet yield anisotropy and, importantly, the attenuation of the spike feature for a long-lived radical pair (10 μs recombination lifetime) subjected to an increasingly strong (fluctuating) field from a nearby nanoparticle. Figure S2 shows the same calculation for a radical pair with the shorter lifetime of 1 μs . When the strength of the nanoparticle field reaches 400 μT , the singlet yield anisotropy is reduced to approximately 10% of its original value, which we will take as a good indication that the compass has been ‘sufficiently disrupted’.

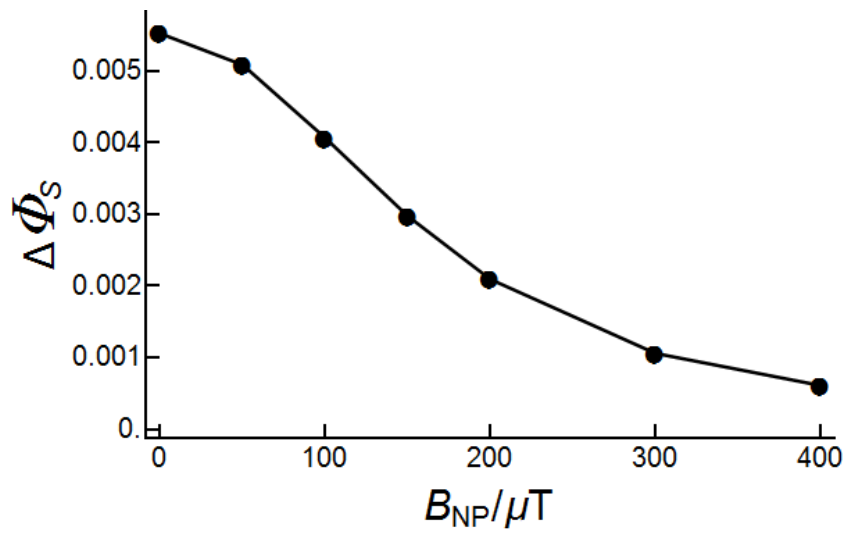


Figure S2. The singlet yield anisotropy, $\Delta\Phi_s$, of the flavin-tryptophan radical pair in cryptochrome as a function of the local field strength produced by a nearby radical. The recombination lifetime of the radical pair was 1 μs . The Earth’s field strength is 50 μT . Both radicals were subjected to a periodically reversing local field in the range 0 to 400 μT . The mean time between field-reversals, τ_N , was 1 ns.

S6. Orientation sampling

To model realistic experimental conditions in which neither the orientation of the radical pair or the nanoparticle can be controlled, the values of singlet yield given in Figure 4 of the main text are an average over a random sample of 500 different orientations of the nanoparticle relative to the applied magnetic field. Due to the isotropic nature of the hyperfine interactions used in these calculations, the orientation of either field relative to the radical pair does not need to be considered. The average singlet yield is calculated as

$$\bar{\Phi}_s = \frac{1}{N} \sum_{i=1}^N \Phi_s(\chi_i, \psi_i),$$

where χ_i and ψ_i are polar and azimuthal angles describing the orientation of the complex. Sample orientations were chosen using

$$\chi_i = \cos^{-1}(2v - 1); \quad \psi_i = 2\pi u,$$

where v and u are random variables uniformly distributed on $[0,1]$. This procedure ensures that all possible orientations of the complex are sampled with equal probability.

S7. Simulations of an intermolecular radical pair reaction *in vitro*

Some model systems for *in vitro* studies of radical pair compass systems are based on intermolecular radical pair reactions. For these systems, only one of the radicals, bound to the magnetoferritin nanoparticle would feel the field of the nanoparticle. Figure S3. shows the simulated MARY curves for such a reaction, where the nanoparticle is bound to the tryptophan radical. The results are similar, if slightly less pronounced, to those shown in Figure 4 of the main text.

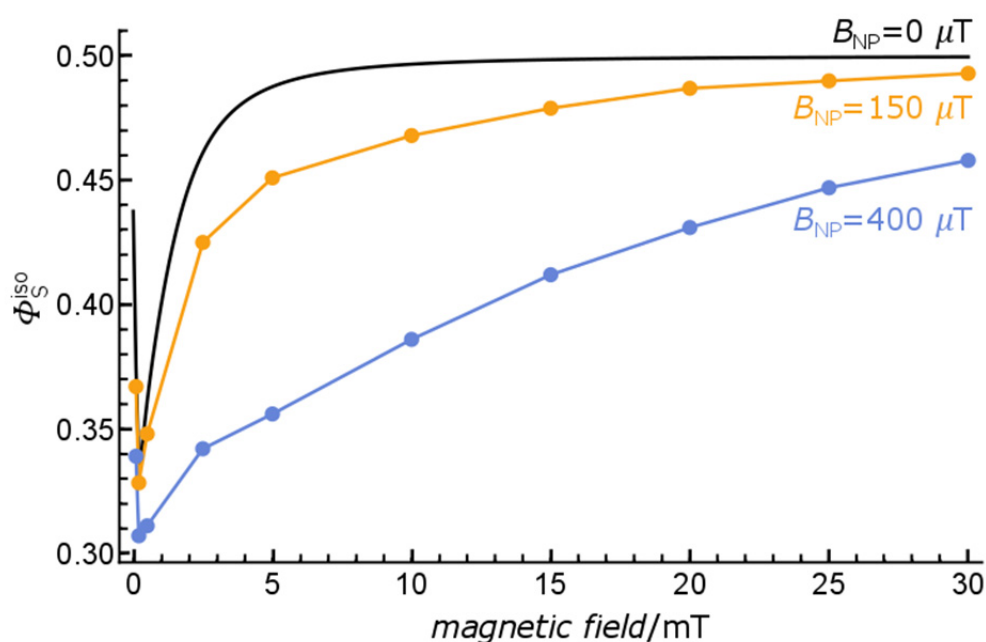


Figure S3. The singlet yield Φ_S^{iso} as a function of the strength of an applied magnetic field, B_0 , for a model flavin-tryptophan radical pair containing only the isotropic components of the hyperfine tensors. The presence of a nanoparticle creates a 150 μT or 400 μT field at the radical pair (blue and orange lines, respectively). This field is averaged over 500 randomly chosen orientations of the nanoparticle. The solid black line is the singlet yield in the absence of a nanoparticle. For the averaged data, the singlet yield was only calculated at the marked points, due to the length of the calculation. The field of the nanoparticle is experienced only by the TrpH^{*+} radical. The radical pair recombination lifetime is 1 μs . The Néel relaxation time of the nanoparticle is 1 ns.

References

1. Lee AA, Lau JCS, Hogben HJ, Biskup T, Kattnig DR, Hore PJ. 2014 Alternative radical pairs for cryptochrome-based magnetoreception. *J. R. Soc. Interface* **11**, 20131063. (doi:10.1098/rsif.2013.1063)
2. Kattnig DR, Evans EW, Déjean V, Dodson CA, Wallace MI, Mackenzie SR, Timmel CR, Hore PJ. 2016 Chemical amplification of magnetic field effects relevant to avian magnetoreception. *Nat. Chem.* **8**, 384–391. (doi:10.1038/nchem.2447)
3. Frisch MJ *et al.* 2004 Gaussian 03.
4. Zoltowski BD, Vaidya AT, Top D, Widom J, Young MW, Crane BR. 2011 Structure of full-length *Drosophila* cryptochrome. *Nature* **480**, 396–9. (doi:10.1038/nature10618)
5. Levy C *et al.* 2013 Updated structure of *Drosophila* cryptochrome. *Nature* **495**, E3–E4. (doi:10.1038/nature11995)